

Manipulator and Object Tracking for In Hand Model Acquisition

Michael Krainin, Peter Henry, Xiaofeng Ren, and Dieter Fox

Abstract—Recognizing and manipulating objects is an important task for mobile robots performing useful services in everyday environments. While existing techniques for object recognition related to manipulation provide very good results even for noisy and incomplete data, they are typically trained using data generated in an offline process. As a result, they do not enable a robot to acquire new object models as it operates in an environment. In this paper, we develop an approach to building 3D models of unknown objects based on a depth camera observing the robot’s hand while moving an object. The approach integrates both shape and appearance information into an articulated ICP approach to track the robot’s manipulator and the object. Objects are modeled by sets of surfels, which are small patches providing occlusion and appearance information. Experiments show that our approach provides very good 3D models even when the object is highly symmetric and lacking visual features and the manipulator motion is noisy.

I. INTRODUCTION

The ability to recognize and manipulate objects is an important task for mobile robots performing useful services in everyday environments. Over the last years, various research groups have made substantial progress in recognition and manipulation of everyday objects [22, 6, 2, 5, 14, 21, 9]. While the developed techniques are often able to deal with noisy data and incomplete models, they still have limitations with respect to their usability in long term robot deployments in realistic environments. One crucial limitation is due to the fact that the parameters of the object recognition algorithms are either set manually or trained using offline machine learning techniques. As a result, there is no provision for enabling a robot to autonomously acquire new object models as it operates in an environment. This is an important limitation, since no matter how extensive the training data, a robot might always be confronted with a novel object (type) when operating in an unknown environment.

The goal of our work is to develop techniques that enable robots to autonomously acquire models of unknown objects. Ultimately, such a capability will allow robots to actively investigate their environments and learn about objects in an incremental way, adding more and more knowledge over time. In addition to shape and appearance information, object models could contain information such as the weight, type, typical location, or grasp properties of the object. Equipped with these techniques, robots can become experts in their respective environments and share information with other robots, thereby allowing for rapid progress in robotic capabilities.

M. Krainin, P. Henry, and D. Fox are with the Department of Computer Science & Engineering, University of Washington, Seattle, WA 98195, USA [mkrainin](mailto:mkrainin@cs.washington.edu), [peter_henry](mailto:peter_henry@cs.washington.edu), fox@cs.washington.edu

X. Ren is with the Intel Labs Seattle, Seattle, WA 98195, USA xren@intel.com

D. Fox is also with the Intel Labs Seattle, Seattle, WA 98195, USA



Fig. 1. Experimental setup. We used a WAM arm with BarrettHand on a Segway base. Mounted next to the arm on a pan-tilt unit is a depth camera.

In this paper, we present a first step toward this goal. Specifically, we develop an approach to building a 3D surface model of an unknown object based on data collected by a depth camera observing the robot’s hand moving an object. In contrast to existing work in 3D object modeling [18, 7], our approach does not require a highly accurate depth sensor or a static or unobstructed view of the object. We develop a Kalman filter that uses depth and visual information to track the configuration of the robot’s manipulator along with the object in the robot’s hand. By doing so, our approach can compensate for noise in the manipulator’s joint sensors and provide an accurate estimate for the trajectory of the object. Over time, an increasingly complete 3D model of the object is generated by extracting points from each depth scan and aligning them according to the tracked hand and object position. To improve the shape consistency of the resulting model, we incorporate both shape and visual features into the scan alignment process. The approach integrates the scans into a consistent surface model using surfels, small discs which represent local surface patches [10, 25]. Experiments show that our approach can generate good models even for objects that are highly symmetric, such as coffee cups, and objects lacking visual texture.

Our work provides the following contributions. We develop a Kalman filter based framework for tracking a robot manipulator and an unknown object grasped by the hand. We show how a 3D model of the object can be generated as part of the tracking algorithm. We develop a novel version of articulated ICP that incorporates uncertainty estimates from the Kalman filter, correspondences from visual feature matching, and occlusion information from the surfel model. Finally, we demonstrate first results with an end-to-end system, capable of grasping unknown objects, acquiring a model of the object, and placing it back on a table. We also show that our technique is capable of resuming modeling after the object is placed down and regrasped.

This paper is organized as follows. In the next section, we first describe our Kalman filter approach to tracking a

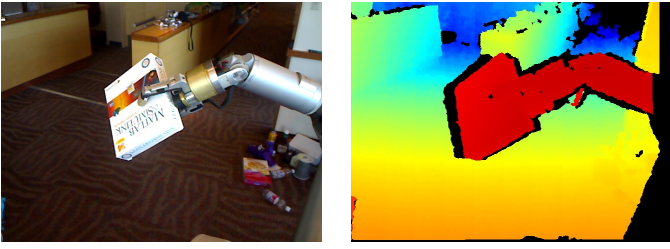


Fig. 2. (left) A Barrett Hand holding a box. (right) Rendering of the depth map provided by our depth camera.

robot’s manipulator and an object grasped by the hand. We then introduce an extension to ICP for articulated objects that can be readily incorporated into our tracking approach. We then go into detail on the modeling process in Section III. Then, in Section IV, we discuss related work, followed by experimental results. Finally, we conclude in Section VI.

II. JOINT MANIPULATOR AND OBJECT TRACKING

Our goal is to acquire 3D models of objects grasped by a robot’s manipulator. To do so, we assume that the robot is equipped with a 3D depth sensor that observes the robot’s manipulation space, producing 3D, colored point-clouds of the robot’s manipulator and the object grasped by the hand. Fig. 2 shows an example image along with depth information of a BarrettHand holding a box. To use such a point cloud for tracking, we assume that the robot has a 3D model of its manipulator. Such a model can either be generated from design drawings or measured in an off line process. The 3D model allows us to generate an expected point cloud measurement for any configuration of the manipulator. In our current system, we use a one-time ray-tracing on an existing model of the WAM Arm and BarrettHand included with OpenRAVE.

A. Kalman Filter Tracking and Object Generation

We will now show how to use a sequence of 3D point clouds and camera images to jointly track a robot’s manipulator and build a model of the object in the robot’s hand.

We use a Kalman filter to track three components in the state vector $\mu = \langle \hat{\theta}, \hat{T}_{calib}, \hat{T}_{obj} \rangle$:

- The manipulator joint angles $\hat{\theta}$.
- The transformation \hat{T}_{calib} , representing an adjustment to the initial camera calibration, which transforms the base of the manipulator into the 3D sensor frame.
- The transformation \hat{T}_{obj} , representing an adjustment to the location of the object relative to the palm of the hand. It transforms the object point cloud into the reference frame of the palm.

The adjustment transformations \hat{T}_{calib} and \hat{T}_{obj} are initialized to identity transformations and are encoded as quaternions and translations. The initial state of the Kalman filter has associated with it a covariance matrix representing the uncertainties in the initial angles, the camera calibration, and the placement of the palm relative to the first object point-cloud. The algorithm, explained below, is shown in Table I.

The algorithm takes as input μ_{k-1} and Σ_{k-1} , namely the previous time mean and covariance of the joint angles, depth

1:	Hand.object.tracker ($\mu_{k-1}, \Sigma_{k-1}, \mathcal{S}_m, \mathcal{S}_{obj}, \mathcal{P}_z, \tilde{\theta}_k, \tilde{\theta}_{k-1}$);
2:	$\mathbf{u}_k = \tilde{\theta}_k - \tilde{\theta}_{k-1}$
3:	$\bar{\mu}_k = \mu_{k-1} + \mathbf{B}\mathbf{u}_k$
4:	$\bar{\Sigma}_k = \Sigma_{k-1} + \mathbf{R}_k$
5:	$\hat{\mu}_k = \text{Articulated_ICP}(\mathcal{S}_m, \mathcal{S}_{obj}, \mathcal{P}_z, \bar{\mu}_k, \bar{\Sigma}_k)$
6:	$\mathcal{S}'_{obj} = \text{Segment_and_merge_object}(\mathcal{S}_m, \mathcal{S}_{obj}, \mathcal{P}_z, \hat{\mu}_k)$
7:	$\mathbf{K}_k = \bar{\Sigma}_k + (\bar{\Sigma}_k + \mathbf{Q}_k)^{-1}$
8:	$\mu_k = \bar{\mu}_k + \mathbf{K}_k(\hat{\mu}_k - \bar{\mu}_k)$
9:	$\Sigma_k = (I - \mathbf{K}_k)\bar{\Sigma}_k$
10:	<i>return</i> $\mu_k, \Sigma_k, \mathcal{S}'_{obj}$

TABLE I

KALMAN FILTER FOR JOINT MANIPULATOR AND OBJECT TRACKING.

sensor calibration, and object position relative to the palm. Additionally, \mathcal{S}_m and \mathcal{S}_{obj} are surfel clouds representing the manipulator and the object respectively. As we will explain in more detail below, surfels describe small patches on the surface of an object, thereby providing more information than pure point clouds. Initially, \mathcal{S}_{obj} is empty since no model of the object is available. $\tilde{\theta}_k$ and $\tilde{\theta}_{k-1}$ are the joint angles reported by the encoders of the manipulator.

As given in Step 2, the motion update \mathbf{u}_k is based upon the difference in reported joint angles since the previous timestep. The prediction step of the Kalman filter then generates the predicted state $\bar{\mu}_k$ in Step 3. The matrix \mathbf{B} simply projects the joint angle update into the higher dimensional space of the Kalman filter state. Associated with this update step is noise in the motion distributed according to the covariance matrix \mathbf{R}_k (Step 4). If the calibration and the object’s position relative to the palm are assumed fixed (that is, if the object is grasped firmly), then \mathbf{R}_k will not contribute any new uncertainty to those parts of the state. Alternatively, one may include those terms in \mathbf{R}_k in order to compensate for movement of the camera or the object inside the hand.

In Step 5, the function *Articulated_ICP* matches the surfel models of the manipulator and object into the observed point cloud and returns an estimate, $\hat{\mu}_k$, of the state vector that minimizes the mis-match between these clouds. Details of this algorithm are given in Section II-C.

Segment_and_merge_object uses the output of *Articulated_ICP* to extract points from the current measurement, \mathcal{P}_z , that belong to the object. To do so, it uses the ICP result $\hat{\mu}_k$ to appropriately transform the manipulator surfel model \mathcal{S}_m into the correct joint angles and into the sensor’s reference frame. \mathcal{S}_m is then used to identify points in \mathcal{P}_z generated by the manipulator via simple distance checking. After segmenting the remaining points in \mathcal{P}_z (which can be done by computing connected components over the image grid, similar to [8]), the points belonging to the object in hand can be identified due to their *physical* relation to the end effector. This technique has the added benefit that it does not require a static background as many vision-based algorithms do. The resulting points are then integrated into \mathcal{S}_{obj} with update rules we will describe

in Section III.

Steps 7 through 9 are standard Kalman filter correction steps, where we take advantage of the fact that *Articulated_ICP* already generates an estimate of the state, $\hat{\mu}_k$, thereby allowing the simplified correction in Step 8. \mathbf{Q}_k represents the uncertainty in the ICP result $\hat{\mu}_k$. While techniques do exist for estimating this matrix (e.g. by using the Jacobian matrix of the error function), they typically make strong assumptions about the correctness of the correspondences. We therefore decided to set \mathbf{Q}_k by hand; a further investigation of estimating uncertainty is left for future work.

In practice, the algorithm requires a reasonably good initialization of the calibration between the depth sensor and the robot manipulator. While we assume that the object is grasped by the hand throughout the entire tracking process, no object model is needed to initialize the filter. Objects in the background are removed based on their spatial relationship to the palm of the robot hand.

B. Articulated ICP

We now describe the function *Articulated_ICP* used in Step 5 of the tracking algorithm. We begin with a review of the ICP algorithm for rigid objects. The input to ICP are two 3D point-clouds, $\mathcal{P}_s = \{p_s^1, \dots, p_s^M\}$ and $\mathcal{P}_t = \{p_t^1, \dots, p_t^N\}$. In our context, \mathcal{P}_s is a combined model of the manipulator and object, and \mathcal{P}_t contains the current observation. The goal is to find a transformation T^* which aligns the point-clouds as follows:

$$T^* = \underset{T}{\operatorname{argmin}} \sum_{i=1}^M \min_{p_t^j \in \mathcal{P}_t} w_i \left| T(p_s^i) - p_t^j \right|^2 \quad (1)$$

To achieve this minimization, the ICP algorithm iterates between the inner minimization of finding correspondences and the outer minimization of finding the transformation minimizing the sum of squared residuals given the correspondences. Since ICP only converges to a local minimum, a good initialization for T is important.

As in [20, 17], the point clouds in our articulated ICP are related to objects that consist of multiple links connected via revolutionary joints. Specifically, each point $p_s^i \in \mathcal{P}_s$ has associated to it a link l_i in the robot's manipulator and is specified in the local coordinate system of that link. Given the set of joint angles, θ , each link l_i in the robot model has a unique transformation T_i^W that maps its points into the reference frame of the depth sensor. The object is treated as its own link, which has an offset T_{obj} from the palm frame. The goal of articulated ICP is to solve for the following:

$$\langle \theta, T_{calib}, T_{obj} \rangle^* = \underset{\langle \theta, T_{calib}, T_{obj} \rangle}{\operatorname{argmin}} \quad (2)$$

$$\sum_{i=1}^M \min_{p_t^j \in \mathcal{P}_t} w_i \left| T_i^W(\langle \theta, T_{calib}, T_{obj} \rangle)(p_s^i) - p_t^j \right|^2$$

Note that in most scenarios, the depth camera is rigidly attached to the robot, in which case the transformation T_{calib} can be estimated offline. Otherwise, the term is included in

the minimization in order to perform calibration at the same time as tracking.

In practice, we have found that the use of point-to-plane type error functions [4], correspondence weights based on agreement of normals, and correspondence distance thresholds can help the performance of articulated ICP. Using point-to-plane requires a non-linear optimizer, for which we use Levenberg-Marquardt.

We compute the correspondence for a surfel using a KD-tree of the point cloud from the depth sensor. As in [25], another option is to simply project each surfel into the image plane and performing bilinear interpolation on the grid structure of the cloud to select corresponding points and normals. In practice, we found that while faster, this approach provides a lower quality of tracking. In particular, it struggles with long, thin objects that may be very close in physical space but do not overlap when projected into the image plane.

For each frame, we extract SIFT keypoints and match them into a cloud of previously seen keypoints on the object. We use RANSAC to ensure geometric consistency and then add these matches as fixed correspondences into our ICP error function. For these feature points, we use a point-to-point error function rather than point-to-plane because it provides a stronger constraint. When, for example, the view of the object consists entirely of a planar surface, the addition of SIFT features as point-to-point matches provides the necessary information to perform the correct within-plane sliding.

In practice, we found it beneficial to bias ICP toward the predicted estimate provided by the Kalman filter. For this, we introduce the Kalman filter state into ICP by adding an additional term to Equation 2 that reflects the state of the Kalman filter: $(\mathbf{x} - \mu)^T \Sigma^{-1} (\mathbf{x} - \mu)$. This bias term is particularly important when there exist ambiguities in the degrees of freedom to adjust due to occlusion or limited field of view. This approach automatically gives preference to adjusting degrees of freedom with higher uncertainty. For example, if the object pose within the hand is fairly certain, matches on the object will result in adjusting the arm pose rather than the object transformation. As a result, holding an object in the hand can actually improve the estimate of the arm pose. It should also be noted that adding this prior has the potential to affect the performance of the Kalman filter. $\hat{\mu}_k$ is supposed to be an independent estimate of the true state, but our prior biases it toward the existing $\bar{\mu}_k$. In practice we find that the benefits of the prior outweigh the risks.

C. Handling Multiple Grasps

We have so far assumed that modeling begins with the object in the manipulator, and at no time is it let go. In Section V-C we will discuss how to achieve this first grasp, but there is another issue as well. The robot's manipulator will occlude parts of the object as shown in Fig. 3, so to get complete models, our algorithm must be able to handle changes in grasp location.

An advantage of performing the object modeling using a robot is that we have knowledge of when it will grasp



Fig. 3. Two grasps of the same object. With just a single grasp, the resulting object model will have holes. Between the two grasps, the entirety of the object is visible.

or release. We use this knowledge to divide our tracking and modeling algorithm shown in Table I in to stages. These stages are: i) the typical object examination stage where the object is being manipulated away from the table’s surface; ii) raising the object from or lowering the object to the table; iii) grasping or releasing; and iv) object on the table.

Stage i is the only stage in which line 6, *Segment_and_merge_object*, is performed. During this stage, there is a strong prior on the object remaining fixed within the manipulator. The object is transformed according to the transformation for the palm link, and the special object link is interpreted as an adjustment to that transformation. Stage ii proceeds exactly as stage i except that the model update is not performed because object segmentation becomes more difficult with other objects in close proximity. Stage iii is treated the same as stage ii except that the prior on object pose is loosened. When the robot grasps or releases an object, the object may move relative to the manipulator. Also possible is that the grasp may fail, and the object could drop. We do not yet address this type of event, but it is clearly a distinct possibility and one worth planning for.

Stage iv is different in that the object is not expected to move with the manipulator. The prior is for the object to remain fixed relative to the robot’s base. The object pose is not changed as the manipulator moves, and the pose adjustment term is reinterpreted to mean an adjustment relative to the robot’s base, not to the manipulator. The combination of these four stages allows the robot to examine an object using one grasp, put the object down, regrasp it, and examine it again, thereby filling in holes from the first grasp. In Section V, we demonstrate an example of a model built from multiple grasps.

III. OBJECT MODELING

We now describe the representation underlying our object models and the key steps involved in updating object models based on new data.

A. Surfels

Our choice of surfels [10, 25] as a representation was strongly influenced by the constraints of our problem. Our depth sensor, while versatile, does suffer from certain types of noise. In particular, we must be able to compensate for quantization errors, filling in of holes, and expansion of objects by extra pixels. An example is shown in Fig. 4. Therefore, it is crucial that we be able to revise the models not just by adding

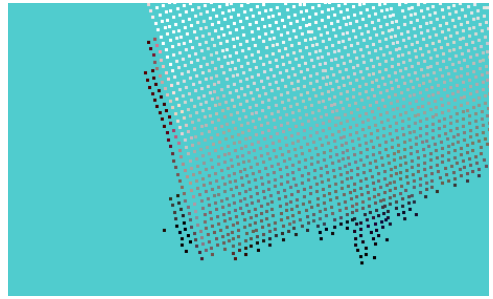


Fig. 4. One of the error modes of our depth sensor. Depicted here is a point cloud of the lip of a mug against a light blue background. Along both edges shown, extra depth points appear and are colored by the scene’s background. Additionally, the sensor has quantization errors and tends to fill in small holes.

points but also by keeping running estimates of their locations and by removing spurious points.

Additionally, the problem at hand involves tracking the robot’s manipulator, some of which may be occluded by the object or itself. We wish to be able to reason explicitly about the visibility of any particular point in \mathcal{S}_m or \mathcal{S}_{obj} before assigning it a correspondence. In doing so, we prevent irrelevant model points from negatively impacting the alignment.

Surfels fit all of these requirements and are very easy to work with. As we explain below, the addition, update, and removal rules for surfels are quite simple and robust. While other representations such as triangle meshes could provide the occlusion information we need, the update rules can be substantially more inefficient because of the need to maintain explicit connections with other vertices. Surfels, on the other hand, can be updated independently of each other and if desired can be later converted to a mesh in a post-processing step.

A surfel is essentially a circular image patch. The properties of a surfel s_i include its position, p_i , its normal, n_i , and its radius, r_i . The radius, as described in [25], is set such that as viewed from the camera position, it would fill up the area of one pixel.

In addition to these required components, one can associate additional attributes to surfels. One attribute in particular is “visibility confidence” c_i . The possible viewing angles of a surfel are divided into 64 bins. The confidence is the number of such bins from which the surfel has been seen at least once. This provides a better measure of confidence than simply the number of frames in which a surfel has been seen because a patch seen from the same angle may consistently produce the same faulty reading. For visualization purposes, we also keep track of the color of the surfel using the frame that has the most perpendicular viewing angle onto the surfel.

B. Model update

After performing the segmentation described in Section II, we use surfel update rules similar to [25] to modify the object model \mathcal{S}_{obj} . Each surfel location p_i is projected into the image plane. We then use bilinear interpolation to determine the point p_i^* and normal n_i^* at that same location in the sensor reading. p_i has a depth d_i and p_i^* has a depth d_i^* ; the difference $d_i - d_i^*$ is

used to determine the update rule that is used. In the following rules, we will say that a sensor reading p_i^* is a valid object reading if its surrounding pixels are in a single object segment, and n_i^* does not deviate from the camera direction by more than θ_{max} .

- 1) $|d_i - d_i^*| \leq d_{max}$: If p_i^* is a valid object reading and n_i^* does not deviate from the camera direction by more than θ_{max} , then the surfel is updated. This is done by computing running averages of the surfel location and normal as well as the grid counter of viewing directions. Additionally, if the new measurement was taken from a closer location, then the radius of the surfel is updated accordingly. If the conditions do not hold, then we do nothing.
- 2) $d_i - d_i^* < -d_{max}$: In this case, the observed point is behind the surfel. If the surfel confidence c_i is below c_{high} , then the existing surfel is considered an outlier and removed. It is replaced by a new one at p_i^* if that is a valid object reading. If c_i is at least c_{high} , then the reading is considered an outlier and is ignored.
- 3) $d_i - d_i^* > d_{max}$: Then the observed point is in front of the model surfel s_i . As suggested by [25] we look to find a surfel that occludes s_i . If we find one, and its confidence is at least c_{high} , and c_i is below c_{high} , then s_i is removed. This is meant to remove surfels that have been erroneously placed in the interior of an object. If no occluding surfel is found, we do nothing.

After surfel update comes the surfel addition step. For each pixel in the object segments, a new surfel is added if there are no existing surfels with normals toward the camera either in front of or close behind the reading. This is a simple heuristic; however, it allows us to acquire models of objects which have two surfaces close together such as the inside and outside of a coffee mug. Finally, there is one more removal step. Any surfel with $c_i < c_{starve}$ that has not been seen within the last t_{starve} frames is removed. This is very effective at removing erroneous surfels without the need to return to a viewing angle capable of observing the surfel patch.

IV. RELATED WORK

The existing work in tracking and modeling address subsets of the problem we are trying to solve; however, no one paper addresses them all. We make use of depth, visual, and encoder information to provide a tracking and modeling solution for enabling active object exploration for personal robotics.

A number of techniques exist for hand-tracking; however, many of these make use of only 2D information such as silhouettes and edge detections [1, 23]. Some require pre-computed databases and may only detect configurations within that database [1] and others are far from real-time algorithms. Given that we are using 3D sensors and that we wish to track the hand in real time through a continuous space of joint angles, such approaches are unsuitable.

Articulated ICP has been used in tracking applications in the past [20, 17]. However, to the best of our knowledge, it has not been integrated with Kalman filters, which provide the

advantages of smoothing and estimating uncertainties. These uncertainties are crucial as they can be fed back into ICP to reflect the accumulated knowledge of the state. Building models of held objects and utilizing them during ICP is also a novel contribution of our algorithm and one which reinforces the need for the Kalman filter.

Typically, object tracking algorithms only rely on the use of visual data or depth data but not both, and to our knowledge none explicitly try to track the hand as a means of improving alignment. In the case of ProFORMA [19], the goal is to acquire and track models via webcam. While visual features alone work fine for some objects, many everyday objects lack sufficient texture for this type of tracking. ProFORMA also uses a different surface representation more suitable to the sparse point clouds produced by structure from motion.

Weise et al. [25] use 3D range scans and model objects using surfels [10] but rely solely on object ICP with projection-based correspondences to provide alignment. They also demonstrate a potentially very useful online loop-closure algorithm. Loop-closure is an issue we have not addressed in this paper but which we plan to implement as future work. This work does not address the issue of hand tracking, an aspect which improves robustness to object symmetries and RANSAC failures.

For the graphics community, obtaining accurate 3D shapes of objects is a primary research objective and has been extensively studied. Many researchers have applied range sensing of various kinds (e.g.[7, 18]) and can recover amazing details by combining meticulous experimental setup with sophisticated geometric inference algorithms, such as that in the Digital Michelangelo Project [15]. In comparison, although we are recovering both object shape and appearance, our objective is not photorealistic rendering, but to robustly and efficiently model objects from an autonomous robot, with an affordable sensor, and to apply such object knowledge in recognition and manipulation.

V. EXPERIMENTS

The robot used in our experiments is shown in Fig. 1. The basic setup consists of a WAM Arm and BarrettHand mounted on a Segway. The depth camera is located to the side and above the robot manipulator so as to provide a good view of the manipulator workspace. The specific depth camera we use was mainly developed for gaming and entertainment applications. The camera provides pixel colors and depth values at 640x480 resolution, at 30 frames per second. The overall quality of the depth data is comparable or slightly better than alternative sensor setups, such as the SwissRanger [11] or the Videre stereo camera with textured light projector prototype developed by Willow Garage [13].

We collected depth camera data and joint angle sequences of the moving system. In all but the last experiments, the manipulator grasps and trajectories were specified manually and the objects were grasped only once. Automatic generation of optimized motion trajectories and multi-step grasping to generate complete object models is discussed briefly in Section V-C. Our current implementation of the algorithm

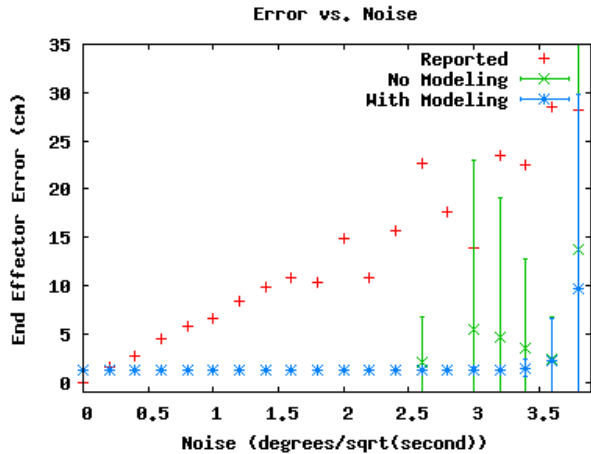


Fig. 5. Distance of the end effector from the ground truth as a function of the per joint angle drift rate. Notice that the tracking error does not increase with noise until at least $2.5^\circ/\sqrt{s}$, and when modeling the object, failures do not begin until $3.4^\circ/\sqrt{s}$.

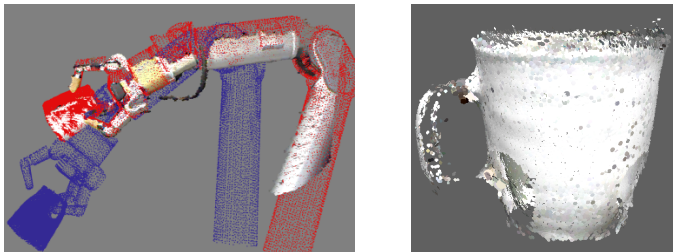


Fig. 6. (left) Drift resulting from $2.0^\circ/\sqrt{s}$ noise. Actual sensor data in true color, tracking result in red, and noisy joint angles in blue. (right) Surfel model produced at this level of noise.

described in Section II-A requires on the order of one second per update step. We are confident that the update rate of the system can be increased to 10 frames per second using a more optimized implementation and taking advantage of GPU hardware. To simulate such a higher update rate, we played back the datasets at approximately one tenth of the real time.

A. Joint Manipulator and Object Tracking

In this experiment, we evaluate the ability of our technique to track the position of the robot hand. Specifically, we investigate if our system would enable accurate tracking of a low cost manipulator equipped with position feedback far less accurate than that of the WAM arm. To do so, we use the WAM controller’s reported angles as ground truth. To simulate an arm with greater inaccuracies, we included normally distributed additive noise of varying magnitude.

To provide an intuitive feel for the units involved, we show in Fig. 6 an example of the deviation between reported and observed manipulator after 20 seconds of motion at a $2.0^\circ/\sqrt{s}$ noise level. In Fig. 5, we demonstrate that our tracking algorithm can handle large amounts of noise in the reported angles without losing accuracy in tracking the end effector. In this experiment, the hand was grasping a coffee mug. Red dots in Fig. 5 show errors for the uncorrected, noisy pose estimates. Green dots, along with 95% confidence



Fig. 7. Shown here are a can and a mug aligned with ICP alone on the left and our algorithm on the right. Due to the high level of symmetry in these objects, ICP is unable to find the correct alignments between depth scans, resulting in useless object models.

intervals, show tracking results when ignoring the object in the robot’s hand. Blue dots are results for our joint tracking approach, when modeling the object and tracking it along with the manipulator. As can be seen, modeling the object further increases the robustness to noise. This is because we can both explicitly reason about the modeled object occluding the fingers and use the object as an additional surface to match. An example model generated for the coffee mug under high noise conditions is shown in Fig. 6. When comparing this model to one built without additional noise (see Fig. 7), it becomes apparent that our approach successfully compensates for motion noise.

B. Object Modeling

In this set of experiments we investigate different aspects of the tracking and object modeling technique.

Many objects in everyday environments exhibit rotational symmetries or are lacking in distinctive geometries for matching. Many existing object modeling algorithms such as [25] rely on being able to geometrically match the object model into the new frame. To demonstrate the advantage of also tracking the manipulator, we show in Fig. 7 how object ICP alone performs on two highly symmetric objects.

In this experiment, object segmentations from the joint ICP were used to produce clouds to be registered, but ICP was left to align the object points without any information about the hand motion. As can be seen in Fig. 7, ICP is unable to recover the proper transformations because of the ambiguity in surface matching. It should also be noted that for the mug case in particular, systems like ProFORMA [19], which rely on tracking visual features would also be incapable of tracking or modeling the object.

We have also found that surfels are a very compact and elegant solution to maintaining object models. Besides the benefits of occlusion-checking and incremental update, it takes many fewer surfels to represent a model than it does points, and the arrangement is cleaner and more visually appealing.

Fig. 8 illustrates the difference between raw data point clouds and surfel models. Shown on the right are the surfel patches belonging to two separate objects. The two panels on the left show the raw, colored point clouds from which the surfels were generated. The raw clouds contained on the

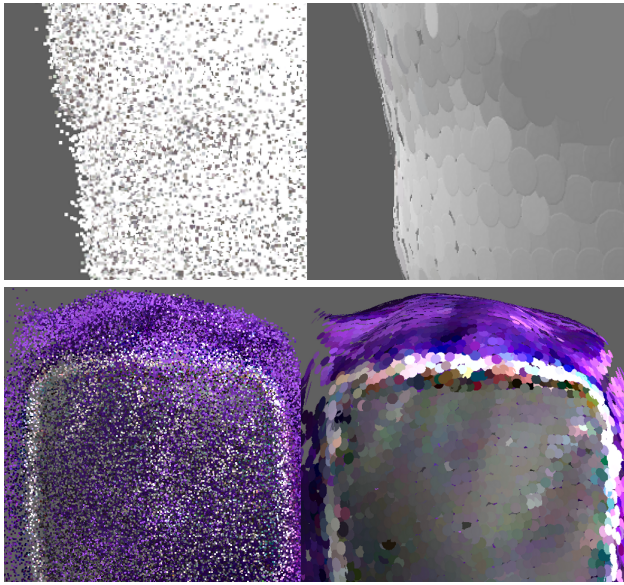


Fig. 8. Comparison between aggregated point clouds and surfel models generated from the same data and the same frame alignments.



Fig. 9. Triangulated surface models constructed from surfel clouds. On the top is a Matlab box and on the bottom a stuffed doll. Any large holes are due to occlusion by the hand.

order of one million points and were randomly downsampled for visualization purposes. The surfel clouds are on the order of ten thousand surfels.

The surfel models we have obtained in our online process contain accurate information of both surface positions and normals, and can be readily used in a post-processing step, through meshing and coloring, to improve the qualities of the shape and visual appearance. We use the open-source Meshlab software and follow a number of standard steps: first we apply the Poisson Reconstruction algorithm [12], with a level of 12, to obtain a surface mesh from the oriented point cloud. Second, we apply the Catmull-Clark subdivision to refine the mesh. Third, we reproject the oriented points to the original frames, and assign vertex colors there. We use the frame that has the most frontal view of a particular vertex, unless it fails to pass a simple color saturation threshold check.

A few of the reconstructed objects are shown in Fig. 9. For rendered videos of the models and videos demonstrating the arm tracking and surfel model construction, see <http://>



Fig. 10. (left) A model of a can constructed using only the first grasp from Fig. 3. Notice the large holes where the hand occludes the view. (right) The same model after the second grasp.

www.youtube.com/user/UWObjectModeling. Also posted there is a video showing the robot’s capability to examine objects while simultaneously driving around.

C. Toward Autonomous Object Modeling

To perform autonomous grasping and modeling, we implemented an approach that enables the robot to pick up an unknown object. The object grasp point and approach direction are determined by first subtracting the object from the table plane using the depth camera data, and then computing the principal component of the point cloud representing the object. The approach is then performed orthogonal to this principal component. While this technique is not intended as a general grasping approach, it worked well enough to perform our initial experiments. Alternatively, one can use local visual or geometric features as in [22] to obtain this first grasp. Once an object is grasped, the manipulator moves it in front of the depth camera in order to construct an object model.

The model can be improved by allowing the robot to place the object back down and regrasp it. We demonstrate this in Fig. 10. While Section II details how the tracking and modeling can be made to work with regrasping, the best way to generate the second grasp is still unclear. Unlike the first grasp, the second grasp can be informed by the mostly complete surfel model. The model can be passed along to a grasp planner (e.g. [2, 16]) but should be done in a way that discourages grasps covering previously unseen areas.

The surfel model can be triangulated as we do above, and holes can be filled using standard hole filling algorithms or by estimating the hidden surface locations based on contact points from the first grasp. One can then incorporate into the grasp quality metric an estimate of the area of newly filled regions hidden by the proposed grasp. Alternatively, one could keep a table of the viewing angles from which the object has been seen and give preference to grasps locations that this table indicates have been seen straight on.

Such a table could also be useful in automatically generating arm trajectories to cover unseen areas of the object. So far we have only been using manually specified arm trajectories. An online selection of trajectories could conceivably provide faster and more complete coverage of objects in addition to adding to the autonomy of the system.

VI. CONCLUSIONS AND FUTURE WORKS

We developed an algorithm for tracking robotic manipulators and modeling objects grasped by a manipulator using depth cameras. Our approach performs tracking, depth sensor calibration, and object modeling all in one Kalman filter based framework. Experiments show that the technique can robustly track a manipulator even when significant noise is imposed on the position feedback provided by the manipulator. The experiments also show that jointly tracking the hand and the object grasped by the hand further increases the robustness of the approach. The insight behind this technique is that even though an object might occlude the robot hand, the object itself can serve as guidance for the pose estimate. We showed that this approach works even while the robot is moving and when there is no initial model of the object available. Tracking accuracy is further improved by incorporating visual features detected on the object into the ICP matching algorithm.

We also introduced a tight integration of the tracking algorithm and an object modeling approach. Our technique uses the Kalman filter estimate to initially locate the object and to incorporate new observations into the object model. We use surfels as the key representation underlying the object and manipulator models. This way, our approach can do occlusion-based outlier rejection and adapt the resolution of the representation to the quality of the available data.

An approach alternative to ours could be to generate an object model by moving a camera around the object. However, this approach cannot provide information about object parts that are not visible based on the object's position in the environment. Furthermore, our approach of investigating an object in the robot's hand also lends itself to extracting information about the object's weight and surface properties.

Our key motivation for this work is in enabling robots to actively investigate objects in order to acquire rich models for future use. Toward this goal, several open research questions need to be addressed. We have discussed possible techniques for initial and subsequent grasp generation, but these problems remain as future work. There is also the problem of automatic trajectory generation for quick coverage of the object. Furthermore, the overall spatial and visual consistency of objects can be further improved by adding loop closure techniques, similar to SLAM mapping [24]. By attaching visual features and grasp information to our object models, a robot could use such models to quickly detect them in the environment, using a technique similar to [3].

ACKNOWLEDGEMENTS

We would like to thank Brian Mayton for all of his assistance, including generating and executing suitable grasps and arm trajectories for our experiments. We would also like to thank Peter Brook for allowing us to incorporate his heuristic grasp planner into our system.

REFERENCES

- [1] V. Athitsos and S. Sclaroff, "Estimating 3d hand pose from a cluttered image," *Computer Vision and Pattern Recognition, IEEE Computer Society Conference on*, vol. 2, p. 432, 2003.
- [2] D. Berenson and S. Srinivasa, "Grasp synthesis in cluttered environments for dexterous hands," in *Proc. of the IEEE-RAS International Conference on Humanoid Robots (Humanoids)*, 2008.
- [3] D. Berenson, S. Srinivasa, D. Ferguson, and J. Kuffner, "Object recognition and full pose registration from a single image for robotic manipulation," in *Proc. of the IEEE International Conference on Robotics & Automation (ICRA)*, 2009.
- [4] Y. Chen and G. Medioni, "Object modelling by registration of multiple range images," *Image Vision Comput.*, vol. 10, no. 3, pp. 145–155, 1992.
- [5] M. Ciocarlie, C. Goldfeder, and P. Allen, "Dimensionality reduction for hand-independent dexterous robotic grasping," in *Proc. of the IEEE/RSJ International Conference on Intelligent Robots and Systems (IROS)*, 2007.
- [6] A. Collet Romea, D. Berenson, S. Srinivasa, and D. Ferguson, "Object recognition and full pose registration from a single image for robotic manipulation," in *Proc. of the IEEE International Conference on Robotics & Automation (ICRA)*, 2009.
- [7] B. Curless and M. Levoy, "A volumetric method for building complex models from range images," in *ACM Transactions on Graphics (Proc. of SIGGRAPH)*, 1996.
- [8] P. F. Felzenszwalb and D. P. Huttenlocher, "Efficient graph-based image segmentation," *Int. J. Comput. Vision*, vol. 59, no. 2, pp. 167–181, 2004.
- [9] J. Glover, D. Rus, and N. Roy, "Probabilistic models of object geometry with application to grasping," in *International Journal of Robotics Research (IJRR)*, vol. 28, no. 8, 2009.
- [10] M. Habbecke and L. Kobbelt, "A surface-growing approach to multi-view stereo reconstruction," in *CVPR*, 2007.
- [11] M. Imaging, "<http://www.mesa-imaging.ch/>."
- [12] M. Kazhdan, M. Bolitho, and H. Hoppe, "Poisson surface reconstruction," in *Symposium on Geometry Processing*, 2006.
- [13] K. Konolige, "Projected texture stereo," in *Proc. of the IEEE International Conference on Robotics & Automation (ICRA)*, 2010.
- [14] K. Lai and D. Fox, "3D laser scan classification using web data and domain adaptation," in *Proc. of Robotics: Science and Systems (RSS)*, 2009.
- [15] M. Levoy, K. Pulli, B. Curless, S. Rusinkiewicz, D. Koller, L. Pereira, M. Ginzton, S. Anderson, J. Davis, J. Ginsberg, J. Shade, and D. Fulk, "The digital michelangelo project: 3d scanning of large statues," in *SIGGRAPH*, 2000.
- [16] A. T. Miller and A. T. Miller, "Graspit!: A versatile simulator for robotic grasping," *IEEE Robotics and Automation Magazine*, vol. 11, pp. 110–122, 2004.
- [17] L. Mündermann, S. Corazza, and T. P. Andriacchi, "Accurately measuring human movement using articulated icp with soft-joint constraints and a repository of articulated models," in *Proc. of the IEEE Computer Society Conference on Computer Vision and Pattern Recognition (CVPR)*, 2007.
- [18] D. Pai, K. van den Doel, D. James, J. Lang, J. Lloyd, J. Richmond, and S. Yau, "Scanning physical interaction behavior of 3d objects," in *ACM Transactions on Graphics (Proc. of SIGGRAPH)*, 2001, pp. 87–96.
- [19] Q. Pan, G. Reitmayr, and T. Drummond, "ProFORMA: Probabilistic Feature-based On-line Rapid Model Acquisition," in *Proc. 20th British Machine Vision Conference (BMVC)*, London, September 2009.
- [20] S. Pellegrini, K. Schindler, , and D. Nardi, "A generalization of the icp algorithm for articulated bodies," in *British Machine Vision Conference (BMVC'08)*, M. Everingham and C. Needham, Eds., September 2008.
- [21] B. Rasolzadeh, M. Bjorkman, K. Huebner, and D. Kragic, "An active vision system for detecting, fixating and manipulating objects in real world," in *International Journal of Robotics Research (IJRR)*, 2009.
- [22] A. Saxena, J. Driemeyer, and A. Ng, "Robotic grasping of novel objects using vision," *International Journal of Robotics Research (IJRR)*, vol. 27, no. 2, 2008.
- [23] E. B. Sudderth, M. I. Mandel, W. T. Freeman, and A. S. Willsky, "Visual hand tracking using nonparametric belief propagation," *Computer Vision and Pattern Recognition Workshop*, vol. 12, p. 189, 2004.
- [24] S. Thrun, W. Burgard, and D. Fox, *Probabilistic Robotics*. Cambridge, MA: MIT Press, September 2005, ISBN 0-262-20162-3.
- [25] T. Weise, T. Wismer, B. Leibe, , and L. V. Gool, "In-hand scanning with online loop closure," in *IEEE International Workshop on 3-D Digital Imaging and Modeling*, October 2009.